Superior nanofiltration membranes with gradient cross-linked selective layer fabricated via controlled hydrolysis

Zi-Ming Zhan[a], Zhen-Liang Xu[a], Ka-Ke Zhu[a], Shuang-Mei Xue[a], Chen-Hao Ji[a], Ben-Qing Huang[a], Chuyang Y. Tang[b], and Yong-Jian Tang[a,*]

[a] *State Key Laboratory of Chemical Engineering, Membrane Science and Engineering R&D Lab, Chemical Engineering Research Center, East China University of Science and Technology, 130 Meilong Road, Shanghai 200237, China*

[b] *Department of Civil Engineering, The University of Hong Kong, Pokfulam HW619B, Hong Kong, China*

ABSTRACT: Nanofiltration (NF) membranes with both high permeability and salt rejection are in dire need for water treatment. Generally, heat treatment is an essential step for fabricating polyamide NF membranes. Conventional heat treatment in an oven causes membrane pore shrinkage and over cross-linking, which often leads to a severe loss of permeation performance. Herein, we report a single-step method by heat-treating membranes in non-neutral solutions to avoid pore shrinkage and generate graded hydrolysis in membrane selective layer. As confirmed by the XPS result, the polyamide NF membrane fabricated via controlled hydrolysis possesses a gradient cross-linking degree vertically along the membrane surface. This optimal polyamide NF membrane had a superior pure water permeability (PWP) of 27.5 L m^{-2} h^{-1} bar^{-1} and high Na_2SO_4 rejection of 98.5%. Such controlled hydrolysis approach provides novel strategy for fabricating high performance polyamide membranes.

Key words: nanofiltration; membrane preparation; hydrolysis; polyamide; permeability

* To whom all correspondence should be addressed.

Email: tangyongjian@ecust.edu.cn; Tel: 86-21-64253670; Fax: 86-21-64252989.

1. Introduction

With the increasing demands for water derived from the rapid development of economy and growth of population, many countries and regions pay more attention to recycling wastewater and using meagre water resources efficiently. Low-cost and effective technologies dealing with wastewater and desalination are in urgent need [1]. Because of its high efficiency and low energy consumption [2], nanofiltration (NF) has been extensively applied in decontaminating wastewater for removing heavy metal ions, separating low-molecular-weight organics and water softening [3, 4]. The pore size of a typical NF membrane is around 1 nm. Compared with reverse osmosis (RO) membranes, NF membranes exhibit high efficiency in separating divalent ions from monovalent ions under lower operating pressure [5]. Currently, thin-film composite (TFC) membrane is the most extensively used form of NF membranes, which is fabricated by interfacial polymerization (IP) on the top of microfiltration or ultrafiltration substrate [6].

A representative polyamide NF membrane is synthesized by interfacial polymerization of an acyl chloride monomer, trimesoyl chloride (TMC), and an amine monomer, piperazine (PIP), at the oil-water interface. The trade-off between permeance and selectivity limits the capacity to increase membrane performance using single materials significantly [4, 7]. Prevailing strategy involves incorporating novel functional materials such as water channel proteins [8-10], metal-organic frameworks (MOF) [11, 12], organic/inorganic nanoparticles [13-15], and carbon-based nanomaterials (e.g., graphene oxide [16-18], and carbon nanotubes [19, 20]) leads to increased water pathways in membrane selective layer. However, these functional nanofillers lead inevitably to complexity and increasing cost in membrane preparations. Some methods are also faced with difficulties in industrialization [4, 21].

Fabricating the polyamide layer with an optimized structure is favored for industry. This strategy involves lowing the thickness or increasing the surface area in a selective layer [22-25]. For example, introducing an interlayer between the substrate and polyamide layer has been shown to reduce the thickness of the polyamide layer and

thus enhance its permeance [26-28]. Greater effective filtration area can be created by the use of sacrificial templates [29, 30] and the creation of nanosized gas bubbles [31]. Wu et al. [27] introduced hybrid interlayer comprising polydopamine and covalent organic framework onto PAN substrate and then the polyamide active layer was fabricated on the interlayer. Owning to excellent hydrophilicity and high porosity of the hybrid interlayer, the thickness of the polyamide active layer was reduced to 11 nm and the resulting NF membrane exhibited outstanding permeability. Jiang et al. [32] developed the aqueous templated onto the surface of the substrate, which resulted in the formation of surface nanostructures on the polyamide NF membrane and simultaneously enlarged the permeable area. The water permeance of the optimal membrane is 21.3 L m^{-2} h^{-1} bar^{-1}. Recently, gradient cross-linked structure for the active layer was reported. Guo et al. [33] fabricated a gradient cross-linked polyvinyl alcohol (PVA) active layer by introducing the crosslinker to the surface of the substrate before PVA coating. Owning to this gradient structure, the water permeance of the optimized membrane was significantly improved. Inspired by this strategy, the gradient cross-linked structure can also be applied in polyamide active layer by controlled hydrolysis. Jun et al. [34] investigated the effect of acid-catalyzed hydrolysis on the performance of a commercial NE70 polyamide membrane. Do et al. [35] reports the possibility of simultaneous enhancement in membrane permeability and rejection by hypochlorite-induced hydrolysis under mild chlorine and alkaline conditions. However, these hydrolysis procedures are generally hard to optimize and the small to moderate improvements in separation properties have been reported (e.g., 10% enhancement in water permeance by acid-catalyzed hydrolysis [34]).

Conventionally, a nascent polyamide membrane is placed in an oven to allow more complete polymerization between the monomers. In our previous research, the influence of heat treatment conditions on polyamide NF membrane performance was systematically investigated [36]. The results show that two accompanying problems, over cross-linking of the polyamide active layer and shrinkage of membrane pores, will inevitably arise from the drying process. Heat treatment in air leads to a great loss of membrane permeability. Consequently, alternative curing strategies need to be

developed to avoid the permeability loss for high-performance polyamide NF membranes.

Herein, we report a single-step method to fabricate polyamide NF membranes with superior performance. Water heat treatment is conducted immediately after fabricating the nascent polyamide NF membrane, which effectively avoids the drawbacks caused by heat treatment in air. More importantly, the adjustment in the pH value of a water bath is applied to control the hydrolysis of membrane selective layer. This single-step method resulting in a gradient cross-linked structure of polyamde active layer, maintaining the fast water pathway and regulating the crosslinking density in the NF membrane. Our study provides a facile and industrially feasible strategy to improve the performance of the NF membrane.

2. Experimental

2.1. Materials

Polyethersulfone (PES, pure water permeability (PWP) =180 L m^{-2} h^{-1} bar^{-1}) was kindly provided by Development Center for the Water Treatment Technology. Inorganic salts, neural organics (glucose, sucrose, raffinose and carbamide, AR), piperazine (PIP, GR), HCl (AR), NaOH (AR), n-hexane (AR), and poly(ethylene glycol) (PEG, AR) were all provided from Sinopharm Chemical Reagent Co., Ltd. Trimesoyl chloride (TMC, ≥98%) used for IP was obtained from Qingdao Benzo Chemical Company.

2.2. Preparation of polyamide NF membrane

According to our previous work [37], IP was conducted to prepare the polyamide NF membranes. The aqueous solutions comprising PIP (1% w/v) and organic solution containing TMC (0.15% w/v) were prepared in advance. Aqueous media used for heat treatment in the pH range of 0-14 was prepared by NaOH and HCl, respectively. The PES membrane as porous support was immersed into DI water for 12 hours before interfacial polymerization. Then the PES membrane was hung up for airing until no visible water droplet. After that, the PES substrate was gripped tightly between two square molds (made by polytetrafluoroethylene). The aqueous solution was added onto

the surface of the PES membrane and kept for 3 min. Then the remaining solution was dumped and the residual droplet was removed by an air knife until no visible water droplet. Subsequently, the organic solution was added onto the wetted substrate to form the polyamide active layer and reacted for 15 s. The nascent polyamide NF membrane was put in DI water with different pH values at 50 °C for 5 min for membrane curing. Meanwhile, partial hydrolysis could occur on the surface of the polyamide active layer under acid or alkaline conditions. In order to maintain the consistency of the same sample, the prepared heat treatment solution was divided into three parts for the identical sample.

As schematically illustrated in **Fig. 1**, the polyamide NF membrane is fabricated on a PES porous support via interfacial polymerization. The aqueous solutions comprising PIP (1% w/v) and an organic solution comprising TMC (0.15% w/v) react at the water-organic interface. After pre-polymerization, the nascent polyamide was heat-treated in the air (80 ºC, which is the optimal condition via heat treatment in oven verified by our previous study [38]) or water (50 ºC). The polyamide NF membranes heat treated in air, neutral aqueous media (pH=7), acid aqueous media (pH=0) and alkaline aqueous media (pH=14) are denoted as PA@A, PA@W-7, PA@W-0, and PA@W-14, respectively.

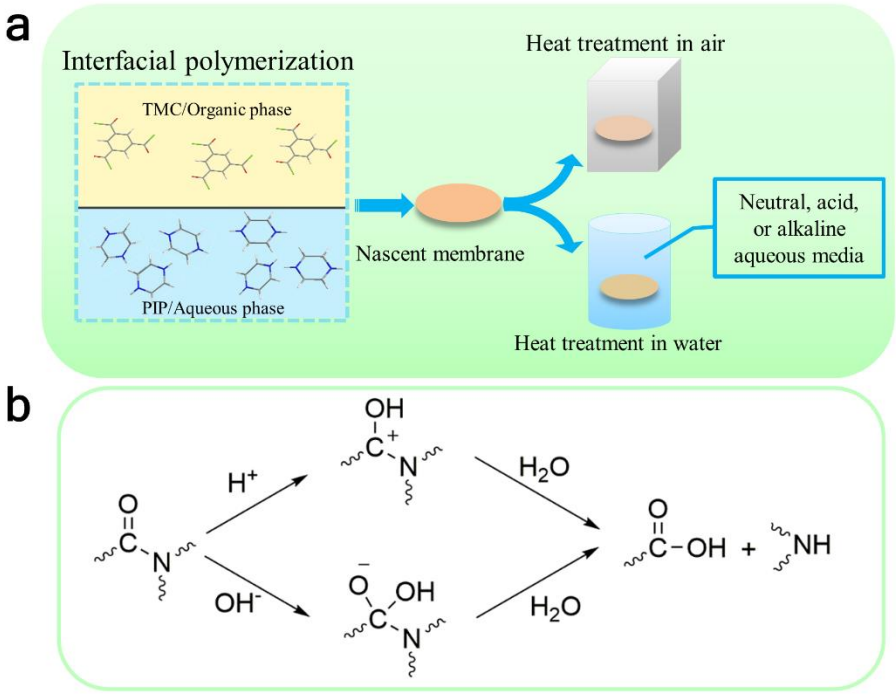

Fig. 1. Schematic diagram of (a) membrane fabrication via different heat treatment process and (b) acid/base-catalyzed amide bond hydrolysis.

2.3. Characterization

XPS was tested by an X-Ray photoelectron spectroscopy (XPS, VG-Miclab II, UK). SEM and AFM images were acquired from a field-emission scanning electron microscope (SEM, NOVA NANOSEM450) and atomic force microscopy (AFM, NanoScope IIIA, USA), respectively. The dynamic water contact angle was obtained on a contact angle meter (JC2000A, ShanghaiZhong Cheng Digital Equipment Co., Ltd., China) at 25 °C. Total organic carbon was acquired from a TOC analyzer (Shimadzu, Model TOCVPN, Japan). Zeta potential was tested with a 1 mM KCl solution from pH 3 to 10 by a potentiometric analyzer (Zeta, SurPASS, Austria).

The rejection experiment of 0.3 g L^{-1} neutral organics (PEG200, 300, 400 and 600, AR) was carried out for the measurement of molecular weight cutoff (MWCO).

2.4. Calculation of polyamide crosslinking density

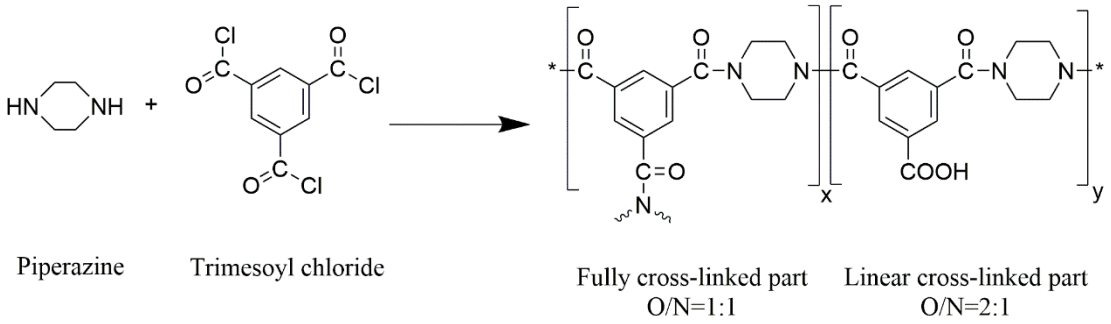

Fig. 2. Interfacial reaction of piperazine with trimesoyl chloride and formation of semi-aromatic polyamide.

Polyamide active layer was fabricated by piperazine and trimesoyl chloride from an interfacial reaction, and the schematic diagram is shown in Fig. 2. From the formation of semi-aromatic polyamide, the O/N ratio can be calculated by Equation (1), where x and y represent fully and linear cross-linked part, respectively. The crosslinking density can be calculated by Equation (2) [25].

$$\frac{O}{N} = \frac{3x+4y}{3x+2y} \quad (1)$$

$$Crosslinking\ \ density = \frac{x}{x+y} * 100\% \quad (2)$$

2.5. NF performance test

The NF performance was measured by a cross-flow filtration rounded module and the area is π×3.0×3.0 cm^2. For the sake of data reliability, three samples prepared by the same conditions were measured by three-module with identical feed solutions. The PWP was determined by Equation (3):

$$\mathrm{PWP} = \frac{V}{A \times t \times P} \quad (3)$$

Where V is permeate volume of the test solution (L), t is the colleting time, A is the effective area for nanofiltration (m^2), and P is the operating pressure (bar). The solute rejection was determined by Equation (4):

$$\mathrm{R}\ (\%) = \left(1 - \frac{C_p}{C_f}\right) \times 100\% \quad (4)$$

Where C_f and C_p are the salt concentration of feed and permeate solution,

respectively. The concentration of feed solutions (NaCl, $MgCl_2$, $MgSO_4$, and Na_2SO_4) is 2000 ppm.

3. Results and discussion

3.1. Surface element composition

Surface element compositions were analyzed by XPS with a photoelectron takeoff angle of 30° and a detection depth around 5 nm. **Table 1** exhibits the surface element composition and crosslinking density of the PA@A, PA@W-7, PA@W-0, and PA@W-14 NF membranes, respectively. The crosslinking density of the polyamide active layer is calculated by the atomic ratio of O and N [25, 39]. The crosslinking density of PA@A, PA@W-7, PA@W-0, and PA@W-14 are 66.7%, 64.3%, 20.6%, and 27.3%, respectively (Table 1). Compared with the typical PA NF membrane previously reported works, the PA@W-0 and PA@W-14 have a much lower crosslinking density [25]. This could be ascribed to the hydrolysis of the polyamide bond caused by the strong acid solution or the strong alkali solution. A similar situation is found in PA@W-14. It is noteworthy that the low crosslinking density can still maintain a high rejection. In order to explore the crosslinking density of the deeper polyamide active layer, the photoelectron takeoff angle was transferred from 30º to 90º, and the corresponding maximum detection depth was changed from 5 nm to 10 nm [40]. The XPS spectra is shown in **Fig. 3**. With the increase of detection depth, the crosslinking density of PA@A and PA@W-7 exhibits a slight difference, yet that of PA@W-0 and PA@W-14 is greatly improved. These results demonstrate that the hydrolysis of polyamide bonds mainly occurred in the top surface of the polyamide active layer. The deeper polyamide active layer may contribute to the high rejection. The top polyamide layer is loose, while the bottom polyamide layer is dense. Such a gradient cross-linked structure has been reported recently [33], and **Fig. 4** shows the cross-sectional structure of the polyamide active layer.

Table 1 The surface element composition and crosslinking density of the polyamide NF membrane (the detection depth is 5 nm)

Sample	Atom percent (%)			O/N	Crosslinking density (%)
	C1s	N1s	O1s		
Binding energy (eV)	284.5	399.5	532.5		
PA@A	72.1	12.4	15.5	1.25	66.7
PA@W-7	71.8	12.4	15.8	1.27	64.3
PA@W-0	69.0	11.4	19.6	1.72	20.6
PA@W-14	70.2	11.3	18.5	1.64	27.3

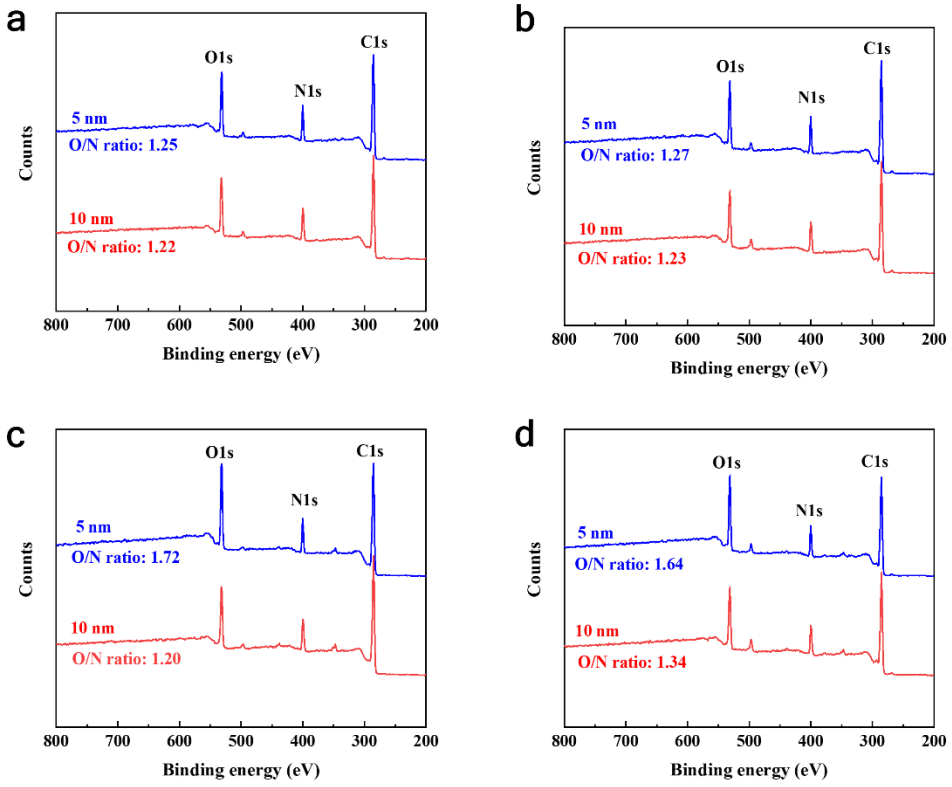

Fig. 3. XPS survey spectra of (a) PA@A, (b) PA@W-7, (c) PA@W-0 and (d) PA@W-14 NF membranes.

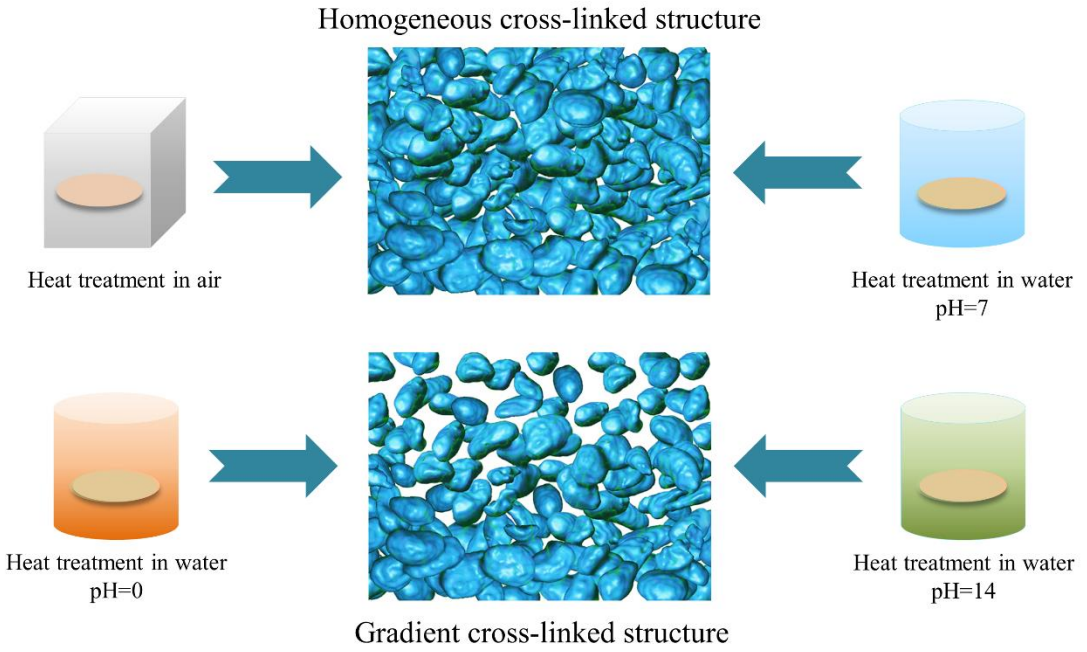

Fig. 4. The cross-sectional structure of the polyamide active layer

3.2. Morphology

The morphology and cross-section of the supporting layer and polyamide membrane are shown in **Fig. 5**. The sponge-like structure can be observed in the cross-section of a supporting layer, which provides a suitable pore size for interfacial polymerization and an required strength for high-pressure operation [41, 42]. The top surface of PA@A, PA@W-0, and PA@14 have a typical nodular appearance [43], and the last two are more obvious. The crumpled structure could be observed on the surface of PA@W-7 active layer. Compared to PA@W-7 NF membrane, PA@A NF membrane has a thinner polyamide layer of 69.3 nm, which may be resulted from the shrinkage of the active layer during heat treatment in air. Although the thickness of PA@W-7 is larger than PA@A, the relatively low crosslinking density causes the flux of PA@W-7 to be higher than PA@A. The dry process will also lead the decline of the flux [36]. Both PA@W-0 and PA@14 have thinner active layers of 53.1 and 57.7 nm, respectively, which are significantly less than that of PA@W-7 due to the controlled hydrolysis. The cross-sectional SEM images of PA@W-0 and PA@W-14 with a magnification of 20,000 are shown in **Fig. S1**.

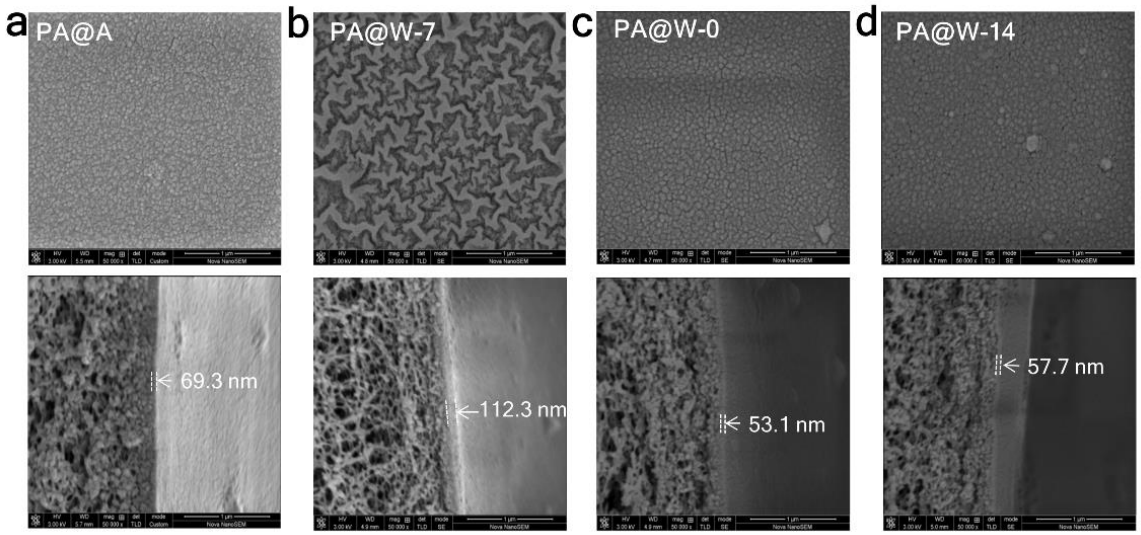

Fig. 5. SEM images of the PA@A, PA@W-7, PA@W-0 and PA@W-14 NF membranes.

3.3. MWCO

The MWCO of different NF membranes is measured by rejecting PEG with different molecular weights (200, 300, 400, and 600 g mol^{-1}). When the rejection of PEG is 90%, the molecular weight of the PEG is defined for the MWCO of NF membrane.[44] The rejection experiment results are exhibited in **Fig. 6**. PA@A NF membrane owns the smallest MWCO of 220 Da, which can be attributed to the over cross-linking of the polyamde active layer and shrinkage of membrane pores.[45] The relatively larger MWCO of PA@W-0 and PA@W-14 can be interpreted to be owing to the amide bond hydrolysis on the surface of the polyamide layer.

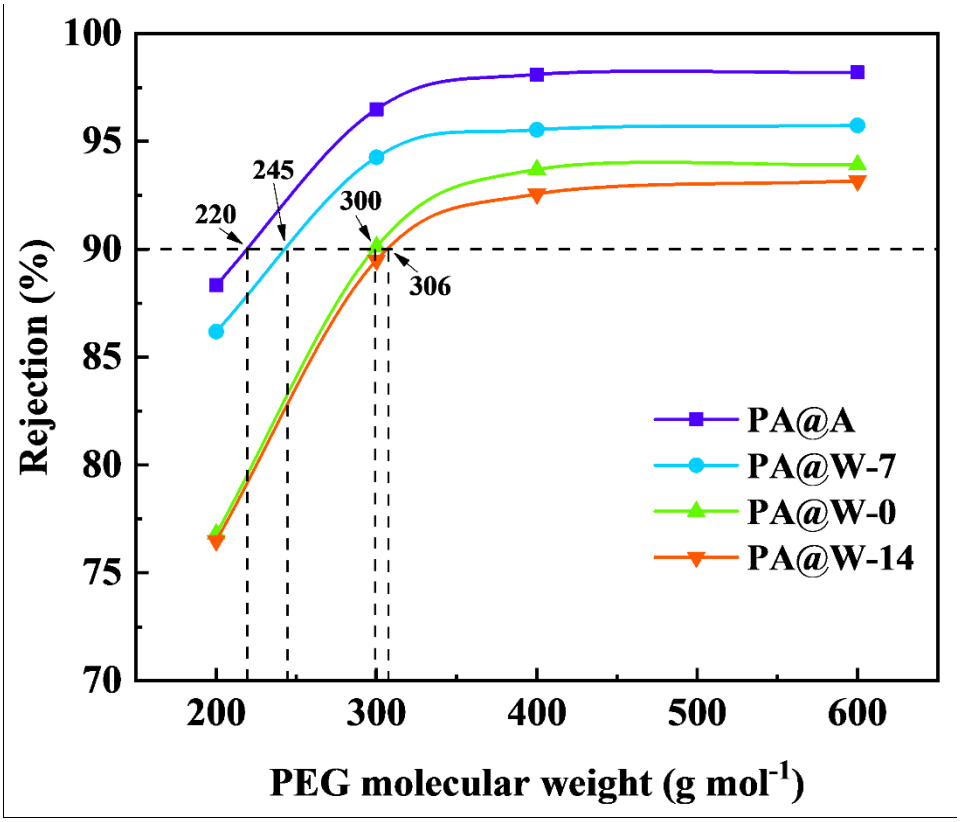

Fig. 6. MWCO of the PA@A, PA@W-7, PA@W-0, and PA@W-14 NF membranes.

3.4. Zeta potential

Zeta potential of the polyamide membrane was tested, and the data was exhibited in **Fig. 7**. Isoelectric point (IEP) of PA@A, PA@W-7, PA@W-0, and PA@W-14 were ~pH 4.4, 3.8, 3.0 and 3.2, respectively. The surface of polyamide layer heat-treated in water (PA@W-7, PA@W-0, and PA@W-14) became more negatively charged, which can be attributed to the negative carboxyl groups hydrolyzed by amide bonds. The schematic diagram of acid/base-catalyzed amide bond hydrolysis could be seen in **Fig. S4** [46, 47]. With the hydrolyzation of amide bonds in strong acid/base conditions, the membranes exhibit a stronger electric density by the generation of carboxyl groups possessed negative charge and amine groups possessed positive charge.

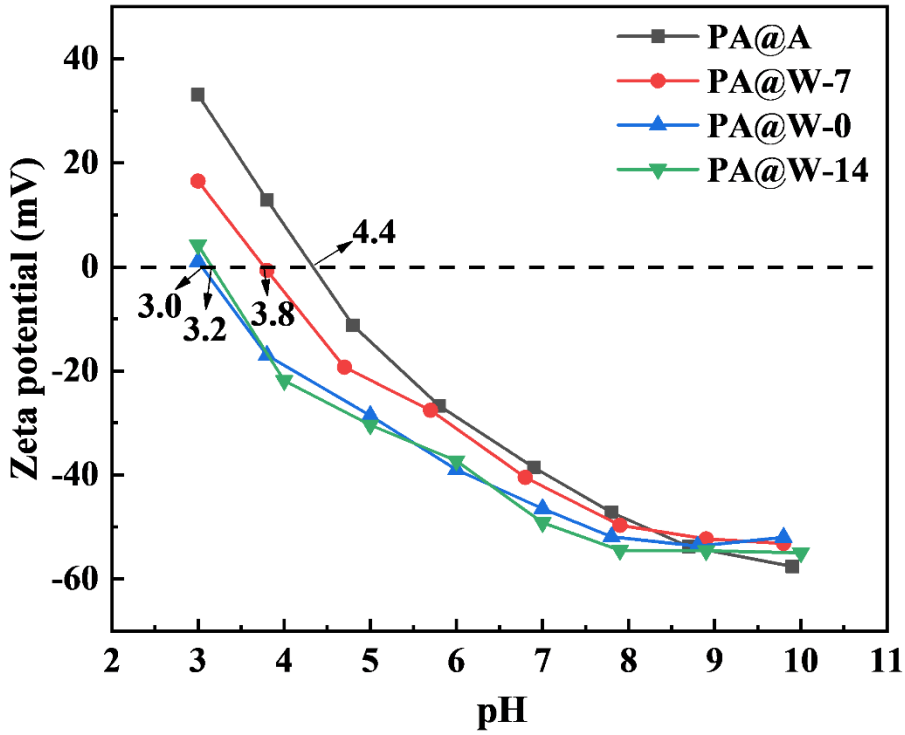

Fig. 7. Zeta potential of PA@A, PA@W-7, PA@W-0, and PA@W-14 NF membranes.

3.5. Nanofiltration performance

The effects of temperature and pH value of the water bath on the nanofiltration performance of the polyamide membrane were studied. The rest of preparation parameters remained unchanged (i.e., PIP (1% w/v) in aqueous solution and TMC (0.15% w/v) in organic solution). **Fig. 8a** shows the variation of PWP and Na_2SO_4 rejection of polyamide NF membranes fabricated by different aqueous solution bath temperatures (40, 50, 60 and 70 ºC). With the increase in temperature, the PWP decreased from 14.0 to 9.8 L m^{-2} h^{-1} bar^{-1} while Na_2SO_4 rejection improved from 93.8% to 97.7%. Hereafter, heat treatment in water at the 50 ºC was chosen for further investigation, as the relatively high flux with a satisfying rejection.

The performance of the NF membrane mainly depends on the thickness, crosslinking density, and microporosity of the thin active layer [10, 48]. To further improve the properties of polyamide membranes, the impact of pH value on the performance of polyamide membrane was also tested. As shown in **Fig. 8b**, when the pH value reduces from 5 to 0, the PWP greatly increases from 10.0 to 27.5 L m^{-2} h^{-1}

bar^{-1} while the Na_2SO_4 rejection keeps at the same level. With the pH value increased from 5 to 14, the PWP sharply improved from 10.0 to 25.5 L m^{-2} h^{-1} bar^{-1}. This enhanced permeability could be explained by the fact that some nascent polyamide fragment is unstable in strong acid or alkali conditions. They will hydrolysis and get removed from the selective layer resulting in extremely low crosslinking density and relatively large MWCO. Meanwhile, the controlled hydrolysis also halves the membrane thickness, which further contributes to the improvement of flux. Meanwhile, the high rejection of Na_2SO_4 could be attributed to the gradient cross-linked structure of the polyamde active layer.

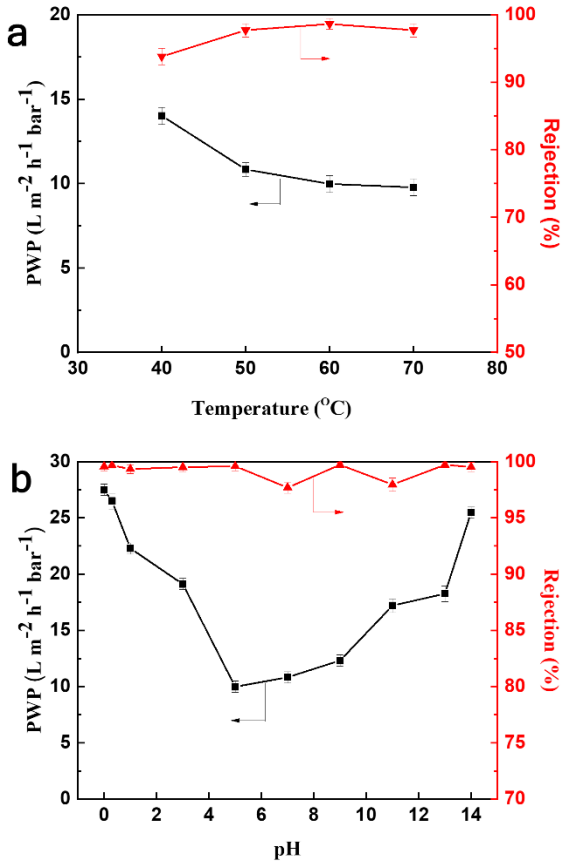

Fig. 8. (a) Effect of treatment temperature of the aqueous media on flux and rejection of polyamide NF membrane, with the pH of the aqueous media maintained at 7. (b) Effect of the pH of the aqueous media on flux and rejection of polyamide NF membrane, with the temperature of the aqueous media fixed at 50 °C. For the performance test, the feed water contained 2000 ppm Na_2SO_4 at an applied pressure of 5 bar.

The impacts of operating pressure on the permeability and salt rejection are also studied with 2 g/L Na_2SO_4 solution. The water flux of PA@A NF membrane increases linearly with operating pressure ranging from 2 to 5 bar but increases slowly at higher operating pressure because of the concentration polarization (**Fig. 9a**) [49]. The concentration polarization is not obvious in the PA@A NF membrane due to its low water flux. Both PA@A and PA@W-0 NF membrane exhibit extremely high Na_2SO_4 rejection of above 99% throughout the operating pressure range, suggesting that defect-free PA active layers were fabricated. In **Fig. 9b**, the PWP of PA@W-0 reaches up to 27.5 L m^{-2} h^{-1} bar^{-1}, which is a five-time increase than that of PA@A. This can be ascribed to the gradient cross-linked structure and relatively large MWCO. The rejections of three polyamde NF membranes for four different salts are measured (**Fig. 9c**). Based on Donnan's exclusion and sieve effect [50], the salt rejection of three polyamide NF membranes follows the order: Na_2SO_4 > $MgSO_4$ > $MgCl_2$ > NaCl, and it is consistent with our previous results [38, 51]. Compared with PA@A, the rejection for $MgCl_2$ and NaCl of PA@W-0 is much higher. This abnormal phenomenon may result from the hydrolyzation of amido bonds during heat treatment in water, which improved the electric density and strength of the Donnan effect.

The PWP and Na_2SO_4 rejection of our membranes (marked as 1-4, representing PA@A, PA@W-7, PA@W-0, and PA@W-14, respectively) are compared with the commercial NF membranes and state-of-art NF membrane reported in the literature (**Fig. 9d**). The optimal polyamide NF membrane in our work (PA@W-0) shows outstanding water permeation and simultaneously maintains a high salt rejection. The long-term test was carried out for 10 days to estimate the stability of the optimal membrane (PA@W-0). As shown in Fig. 10, the optimal membrane exhibits a stable flux behavior around 116.0 L m^{-2} h^{-1}, while the Na_2SO_4 rejection maintains over 98.0%. This indicated that the polyamide membranes optimized by this novel strategy possess a great stability, which hold great promise in industrial applications.

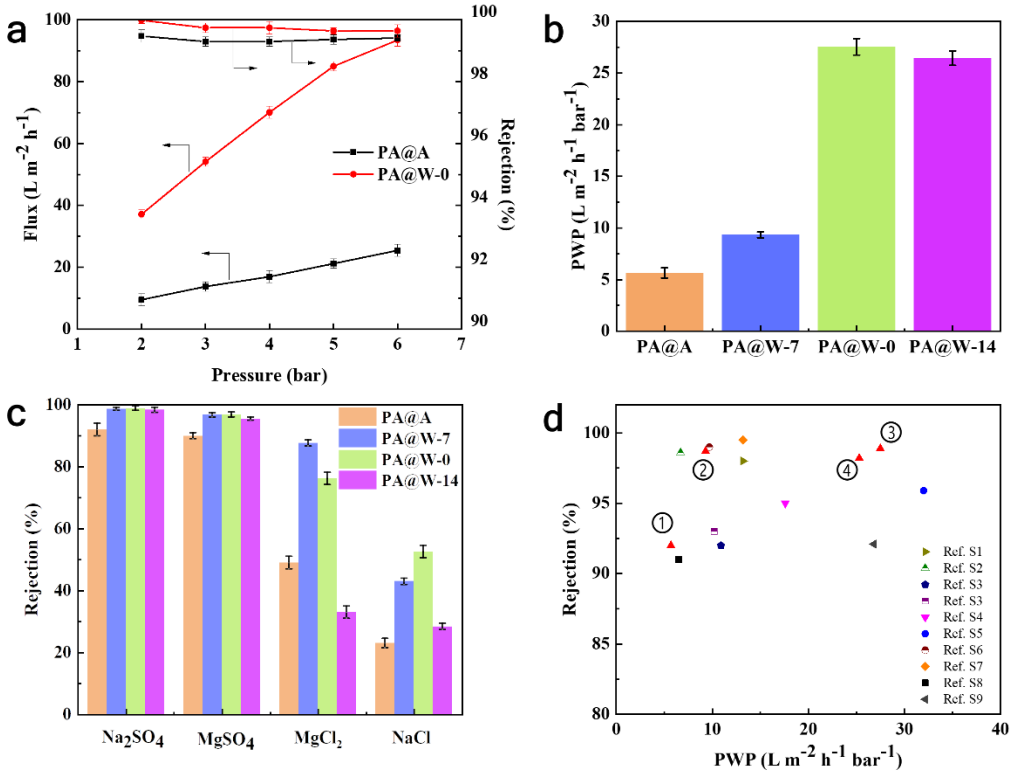

Fig. 9. (a) Impact of operational pressure on the properties of PA@A and PA@W-0 NF membranes. (b, c) Variation of flux and rejection of the resulting membranes (d) Comparison with other state-of-art nanofiltration membranes reported in papers in terms of PWP and rejection for Na_2SO_4. (① PA@A ②PA@W-7 ③PA@W-0 ④PA@W-14). The feed water contained 2000 ppm Na_2SO_4. Unless specified otherwise, the applied pressure was 5 bar.

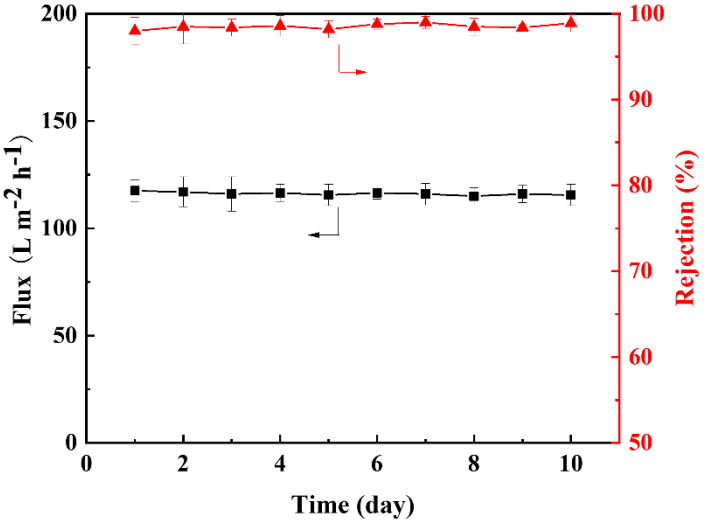

Figure 10. Long-term test of the optimal NF membrane (PA@W-0) during 10 days (5 bar, 25 °C, 2000 ppm Na_2SO_4).

4. Conclusion

In this work, we have developed a facile strategy to NF membranes with gradient cross-linking polyamde layer for enhanced NF performance. Heat treatment in water is

carried out, which effectively avoids the over cross-linking and shrinkage of water pathways in a polyamde active layer compared to conventional heat treatment in air. With the hydrolysis of amido bond adjusted by the strong acid solution or the strong alkali solution, the polyamide NF membrane with gradient cross-linked structure are fabricated. The performance of the polyamide NF membrane can be controlled easily by adjusting the pH value of aqueous media during heat treatment. Additionally, the optimal polyamide NF membrane with PWP of 27.5 L m^{-2} h^{-1} bar^{-1} is obtained. In summary, a facile and effective method to fabricate polyamide membrane with high flux and satisfactory bivalent salt rejection has been offered, which gives implementable perspectives for amplification in the industrial process.

Acknowledgement

This work was financially supported by the National Natural Science Foundation of China (Grant No: 21808060), the Fundamental Research Funds for the Central Universities (222201814009).

REFERENCES

[1] M. Elimelech, W.A. Phillip, The future of seawater desalination: energy, technology, and the environment, Science 333 (2011) 712-717.

[2] M.A. Shannon, P.W. Bohn, M. Elimelech, J.G. Georgiadis, B.J. Mariñas, A.M. Mayes, Science and technology for water purification in the coming decades, Nature 452 (2008) 301-310.

[3] W.J. Lau, G. Stephen, T. Matsuura, ., D. Emadzadeh, ., C. J Paul, A.F. Ismail, A review on polyamide thin film nanocomposite (TFN) membranes: history, applications, challenges and approaches, Water. Res. 80 (2015) 306-324.

[4] A.W. Mohammad, Y.H. Teow, W.L. Ang, Y.T. Chung, D.L. Oatley-Radcliffe, N. Hilal, Nanofiltration membranes review: recent advances and future prospects, Desalination 356 (2015) 226-254.

[5] D. Li, H. Wang, Smart draw agents for emerging forward osmosis application, J. Mater. Chem. A. 1 (2013) 14049-14060.

[6] D. Rana, Y. Kim, T. Matsuura, H.A. Arafat, Development of antifouling thin-film-composite membranes for seawater desalination, J. Membr. Sci. 367 (2011) 110-118.

[7] Z. Yang, H. Guo, C.Y. Tang, The upper bound of thin-film composite (TFC) polyamide membranes for desalination, J. Membr. Sci. 590 (2019) 117297.

[8] Y. Zhao, C.Q. Qiu, X.S. Li, A. Vararattanavech, W.M. Shen, J. Torres, C. Helix-Nielsen, R. Wang, X. Hu, A.G. Fane, C.Y. Tang, Synthesis of robust and high-performance aquaporin-based biomimetic membranes by interfacial polymerization-membrane preparation and RO performance characterization,

J. Membr. Sci. 423 (2012) 422-428.
[9] C.Y. Tang, Z.N. Wang, I. Petrinic, A.G. Fane, C. Helix-Nielsen, Biomimetic aquaporin membranes coming of age, Desalination 368 (2015) 89-105.
[10] Y.X. Shen, W.C. Song, D.R. Barden, T.W. Ren, C. Lang, H. Feroz, C.B. Henderson, P.O. Saboe, D. Tsai, H.J. Yan, P.J. Butler, G.C. Bazan, W.A. Phillip, R.J. Hickey, P.S. Cremer, H. Vashisth, M. Kumar, Achieving high permeability and enhanced selectivity for Angstrom-scale separations using artificial water channel membranes, Nat. Commun. 9 (2018) 2294.
[11] S. Sorribas, P. Gorgojo, C. Tellez, J. Coronas, A.G. Livingston, High flux thin film nanocomposite membranes based on metal-organic frameworks for organic solvent nanofiltration, J. Am. Chem. Soc. 135 (2013) 15201-15208.
[12] N.X. Wang, T.J. Liu, H.P. Shen, S.L. Ji, J.R. Li, R. Zhang, Ceramic tubular MOF hybrid membrane fabricated through in situ layer-by-layer self-assembly for nanofiltration, Aiche. J. 62 (2016) 538-546.
[13] Y. Cheng, Y. Ying, S. Japip, S.D. Jiang, T.S. Chung, S. Zhang, D. Zhao, Advanced porous materials in mixed matrix membranes, Adv. Mater. 30 (2018) 1802401.
[14] M.B.M.Y. Ang, J.M. Pereira, C.A. Trilles, R.R. Aquino, S.-H. Huang, K.R. Lee, J.Y. Lai, Performance and antifouling behavior of thin-film nanocomposite nanofiltration membranes with embedded silica spheres, Sep. Purif. Technol. 210 (2019) 521-529.
[15] D. Hu, Z.L. Xu, C. Chen, Polypiperazine-amide nanofiltration membrane containing silica nanoparticles prepared by interfacial polymerization, Desalination 301 (2012) 75-81.
[16] S. Sajjad, S.A. Khan Leghari, A. Iqbal, Study of graphene oxide structural features for catalytic, antibacterial, gas sensing, and metals decontamination environmental applications, ACS Appl. Mater. Interfaces 9 (2017) 43393-43414.
[17] S. Bano, A. Mahmood, S.J. Kim, K.H. Lee, Graphene oxide modified polyamide nanofiltration membrane with improved flux and antifouling properties, J. Mater. Chem. A. 3 (2015) 2065-2071.
[18] S.M. Xue, C.H. Ji, Z.L. Xu, Y.J. Tang, R.H. Li, Chlorine resistant TFN nanofiltration membrane incorporated with octadecylamine-grafted GO and fluorine-containing monomer, J. Membr. Sci. 545 (2018) 185-195.
[19] A. Tiraferri, C.D. Vecitis, M. Elimelech, Covalent binding of single-walled carbon nanotubes to polyamide membranes for antimicrobial surface properties, ACS Appl. Mater. Interfaces 3 (2011) 2869-2877.
[20] S.M. Xue, Z.L. Xu, Y.J. Tang, C.H. Ji, Polypiperazine-amide Nanofiltration membrane modified by different functionalized multiwalled carbon nanotubes (MWCNTs), ACS Appl. Mater. Interfaces 8 (2016) 19135-19144.
[21] Y.L. Ji, W.J. Qian, Y.W. Yu, Q.F. An, L.F. Liu, Y. Zhou, C.J. Gao, Recent developments in nanofiltration membranes based on nanomaterials, Chin. J. Chem. Eng. 25 (2017) 1639-1652.
[22] B. Yuan, C. Jiang, P. Li, H. Sun, P. Li, T. Yuan, H. Sun, Q.J. Niu, Ultrathin polyamide membrane with decreased porosity designed for outstanding water-softening performance and superior antifouling properties, ACS Appl. Mater. Interfaces 10 (2018) 43057-43067.
[23] P. Gorgojo, S. Karan, H.C. Wong, M.F. Jimenez-Solomon, J.T. Cabral, A.G. Livingston, Ultrathin polymer films with intrinsic microporosity: anomalous solvent permeation and high flux membranes, Adv. Funct. Mater. 24 (2014) 4729-4737.
[24] X.H. Ma, Z. Yang, Z.K. Yao, H. Guo, Z.L. Xu, C.Y.Y. Tang, Interfacial polymerization with electrosprayed microdroplets: toward controllable and ultrathin polyamide membranes, Environ. Sci. Technol. Lett. 5 (2018) 117-122.

[25] S. Karan, Z.W. Jiang, A.G. Livingston, Sub-10 nm polyamide nanofilms with ultrafast solvent transport for molecular separation, Science 348 (2015) 1347-1351.
[26] Y. Zhu, W. Xie, S. Gao, F. Zhang, W. Zhang, Z. Liu, J. Jin, Single-walled carbon nanotube film supported nanofiltration membrane with a nearly 10 nm thick polyamide selective layer for high-flux and high-rejection desalination, Small 12 (2016) 5034–5041.
[27] M.Y. Wu, J.Q. Yuan, H. Wu, Y.L. Su, H. Yang, X.D. You, R.N. Zhang, X.Y. He, N.A. Khan, R. Kasher, Z.Y. Jiang, Ultrathin nanofiltration membrane with polydopamine-covalent organic framework interlayer for enhanced permeability and structural stability, J. Membr. Sci. 576 (2019) 131-141.
[28] Z. Yang, Z.W. Zhou, H. Guo, Z. Yao, X.H. Ma, X. Song, S.P. Feng, C.Y. Tang, Tannic acid/Fe^{3+} nanoscaffold for interfacial polymerization: toward tnhanced nanofiltration performance, Environ. Sci. Technol. 52 (2018) 9341-9349.
[29] S. Zhang, Y. Liu, D. Li, Q. Wang, F. Ran, Water-soluble MOF nanoparticles modified polyethersulfone membrane for improving flux and molecular retention, Appl. Surf. Sci. 505 (2020) 144553.
[30] Z. Wang, Z. Wang, S. Lin, H. Jin, S. Gao, Y. Zhu, J. Jin, Nanoparticle-templated nanofiltration membranes for ultrahigh performance desalination, Nat. Commun. 9 (2018) 2004.
[31] X.H. Ma, Z.K. Yao, Z. Yang, H. Guo, Z.L. Xu, C.Y.Y. Tang, M. Elimelech, Nanofoaming of polyamide desalination membranes to tune permeability and selectivity, Environ. Sci. Technol. Lett. 5 (2018) 123-130.
[32] C. Jiang, L. Tian, Z. Zhai, Y. Shen, W. Dong, M. He, Y. Hou, Q.J. Niu, Thin-film composite membranes with aqueous template-induced surface nanostructures for enhanced nanofiltration, J. Membr. Sci. 589 (2019) 117244.
[33] M. Guo, S.H. Wang, K.F. Gu, X.X. Song, Y. Zhou, C.J. Gao, Gradient cross-linked structure: towards superior PVA nanofiltration membrane performance, J. Membr. Sci. 569 (2019) 83-90.
[34] B.M. Jun, H.K. Lee, Y.N. Kwon, Acid-catalyzed hydrolysis of semi-aromatic polyamide NF membrane and its application to water softening and antibiotics enrichment, Chem. Eng. J. 332 (2018) 419-430.
[35] V.T. Do, C.Y. Tang, M. Reinhard, J.O. Leckie, Effects of chlorine exposure conditions on physiochemical properties and performance of a polyamide membrane-mechanisms and implications, Environ. Sci. Technol. 46 (2012) 13184-13192.
[36] Z.M. Zhan, Z.L. Xu, K.K. Zhu, Y.J. Tang, How to understand the effects of heat curing conditions on the morphology and performance of polypiperazine-amide NF membrane, J. Membr. Sci. 597 (2020) 117640.
[37] Y.J. Tang, Z.L. Xu, S.M. Xue, Y.M. Wei, H. Yang, Improving the chlorine-tolerant ability of polypiperazine-amide nanofiltration membrane by adding NH_2-PEG-NH_2 in the aqueous phase, J. Membr. Sci. 538 (2017) 9-17.
[38] Y.J. Tang, Z.L. Xu, S.M. Xue, Y.M. Wei, H. Yang, A chlorine-tolerant nanofiltration membrane prepared by the mixed diamine monomers of PIP and BHTTM, J. Membr. Sci. 498 (2016) 374-384.
[39] C.Y.Y. Tang, Y.N. Kwon, J.O. Leckie, Effect of membrane chemistry and coating layer on physiochemical properties of thin film composite polyamide RO and NF membranes I. FTIR and XPS characterization of polyamide and coating layer chemistry, Desalination 242 (2009) 149-167.
[40] X. Kong, Z.L. Qiu, C.E. Lin, Y.Z. Song, B.K. Zhu, L.P. Zhu, X.Z. Wei, High permselectivity hyperbranched polyester/polyamide ultrathin films with nanoscale heterogeneity, J. Mater. Chem. A. 5 (2017) 7876-7884.

[41] G.R. Xu, J.N. Wang, C.J. Li, Strategies for improving the performance of the polyamide thin film composite (PA-TFC) reverse osmosis (RO) membranes: surface modifications and nanoparticles incorporations, Desalination 328 (2013) 83-100.
[42] M. Qasim, M. Badrelzaman, N.N. Darwish, N.A. Darwish, N. Hilal, Reverse osmosis desalination: a state-of-the-art review, Desalination 459 (2019) 59-104.
[43] X.Z. Wei, X. Kong, C.T. Sun, J.Y. Chen, Characterization and application of a thin-film composite nanofiltration hollow fiber membrane for dye desalination and concentration, Chem. Eng. J. 223 (2013) 172-182.
[44] Z. Zhang, G. Kang, H. Yu, Y. Jin, Y. Cao, From reverse osmosis to nanofiltration: precise control of the pore size and charge of polyamide membranes via interfacial polymerization, Desalination 466 (2019) 16-23.
[45] Z. Zhao, J. Zheng, B. Peng, Z. Li, H. Zhang, C.C. Han, A novel composite microfiltration membrane: structure and performance, J. Membr. Sci. 439 (2013) 12-19.
[46] M.F. Pill, A.L.L. East, D. Marx, M.K. Beyer, H. Clausen-Schaumann, mechanical activation drastically accelerates amide bond hydrolysis, matching enzyme activity, Angew. Chem. Int. Ed. 58 (2019) 9787-9790.
[47] B.M. Jun, S.H. Kim, S.K. Kwak, Y.N. Kwon, Effect of acidic aqueous solution on chemical and physical properties of polyamide NF membranes, Appl. Surf. Sci. 444 (2018) 387-398.
[48] M.M. Pendergast, E.M.V. Hoek, A review of water treatment membrane nanotechnologies, Energ. Environ. Sci. 4 (2011) 1946-1971.
[49] R. Guha, B.Y. Xiong, M. Geitner, T. Moore, T.K. Wood, D. Velegol, M. Kumar, Reactive micromixing eliminates fouling and concentration polarization in reverse osmosis membranes, J. Membr. Sci. 542 (2017) 8-17.
[50] M. Zhou, T.J. Kidd, R.D. Noble, D.L. Gin, Supported lyotropic liquid-crystal polymer membranes: promising materials for molecular-size-selective aqueous nanofiltration, Adv. Mater. 17 (2005) 1850-1853.
[51] B.Q. Huang, Z.L. Xu, H. Ding, M.C. Miao, Y.J. Tang, Antifouling sulfonated polyamide nanofiltration hollow fiber membrane prepared with mixed diamine monomers of BDSA and PIP, RSC Adv. 7 (2017) 56629-56637.